Published in "Journal of Geophysical Research: Earth Surface
doi: 10.1002/2014JF003276, 2015"
which should be cited to refer to this work.

Variations in Alaska tidewater glacier frontal ablation, 1985–2013

R. W. McNabb[1], R. Hock[1,2], and M. Huss[3,4]

[1]Geophysical Institute, University of Alaska Fairbanks, Fairbanks, Alaska, USA, [2]Department of Earth Sciences, Uppsala University, Uppsala, Sweden, [3]Laboratory of Hydraulics, Hydrology and Glaciology, ETH Zurich Zurich, Switzerland, [4]Department of Geosciences, University of Fribourg, Fribourg, Switzerland

Abstract Our incomplete knowledge of the proportion of mass loss due to frontal ablation (the sum of ice loss through calving and submarine melt) from tidewater glaciers outside of the Greenland and Antarctic ice sheets has been cited as a major hindrance to accurate predictions of global sea level rise. We present a 28 year record (1985–2013) of frontal ablation for 27 Alaska tidewater glaciers (representing 96% of the total tidewater glacier area in the region), calculated from satellite-derived ice velocities and modeled estimates of glacier ice thickness. We account for cross-sectional ice thickness variation, long-term thickness changes, mass lost between an upstream fluxgate and the terminus, and mass change due to changes in terminus position. The total mean rate of frontal ablation for these 27 glaciers over the period 1985–2013 is 15.11 $\pm$ 3.63 Gt a^{-1}. Two glaciers, Hubbard and Columbia, account for approximately 50% of these losses. The regional total ablation has decreased at a rate of 0.14 Gt a^{-1} over this time period, likely due to the slowing and thinning of many of the glaciers in the study area. Frontal ablation constitutes only ~4% of the total annual regional ablation, but roughly 20% of net mass loss. Comparing several commonly used approximations in the calculation of frontal ablation, we find that neglecting cross-sectional thickness variations severely underestimates frontal ablation.

1. Introduction

Despite comprising less than 1% of all glacier ice on Earth, mountain glaciers and ice caps (those bodies of ice separate from the main Greenland and Antarctic ice sheets) are currently responsible for roughly half of the total cryospheric contribution to sea level rise [*Gardner et al.*, 2013]. Although improvements have been made in recent years, our incomplete understanding of frontal ablation hinders attempts to accurately predict global glacier mass change and to make scenario-based projections of the cryospheric contribution to sea level rise [*Intergovernmental Panel on Climate Change*, 2013]. Recent studies have indicated that frontal ablation and surface mass balance contribute roughly equal shares of the net mass loss from the Greenland Ice Sheet [*Rignot and Kanagaratnam*, 2006; *Rignot et al.*, 2008b; *van den Broeke et al.*, 2009; *Enderlin et al.*, 2014], and frontal ablation is the majority of the mass loss from the Antarctic ice sheets [*Rignot*, 2006; *Rignot et al.*, 2008a]. Owing to the complicated nature of the mechanisms behind both calving and submarine melt, however, accurate models and predictions of frontal ablation do not exist.

Estimates of frontal ablation of glaciers other than the ice sheets are scarce, although some do exist. Studies have shown that frontal ablation is an important component of the mass balance of individual glaciers and ice caps in the Arctic and Antarctic [e.g., *Burgess et al.*, 2005; *Dowdeswell et al.*, 2008; *Moholdt et al.*, 2010; *Nuth et al.*, 2012; *Osmanoglu et al.*, 2013, 2014; *Van Wychen et al.*, 2014]. On a regional level, frontal ablation has been estimated to be approximately 30% of the total net mass loss from the Svalbard archipelago [*Hagen et al.*, 2003; *Błaszczyk et al.*, 2009].

Recent studies, employing a variety of techniques, have shown Alaska glaciers to be significant contributors to global sea level rise, in excess of 0.1 mm a^{-1} [e.g., *Arendt et al.*, 2002; *Meier and Dyurgerov*, 2002; *Meier et al.*, 2007; *Luthcke et al.*, 2008; *Berthier et al.*, 2010; *Dyurgerov*, 2010; *Gardner et al.*, 2013]. Only one study [*Burgess et al.*, 2013] has estimated frontal ablation on a regional level for Alaska, though this estimate is short term (2007–2010) and based on coarse estimates of ice thickness. Since achieving their Little Ice Age maximum extents between A.D. 1750 and 1900, most tidewater glaciers in the region have been retreating, although several have been thickening and advancing in recent decades [*Calkin et al.*, 2001; *Larsen et al.*, 2007; *McNabb and Hock*, 2014].

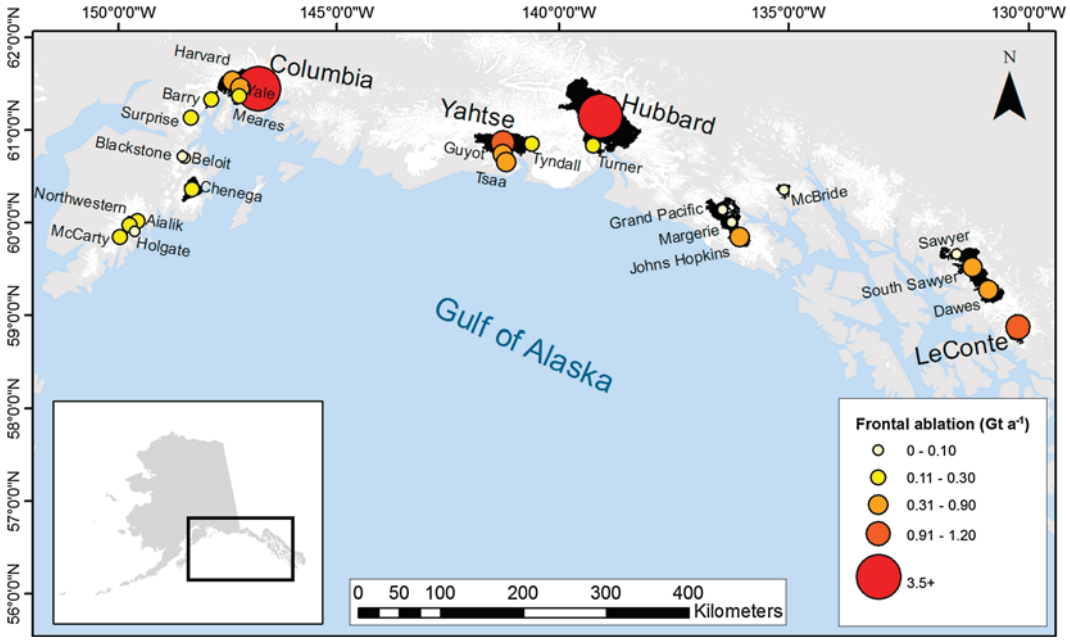

Figure 1. Ice extent (black) and mean frontal ablation rate for the period 1985–2013 for the 27 tidewater glaciers in this study. Other glaciers in the region are shown in white.

In order to investigate the importance of frontal ablation to Alaska tidewater glaciers, this study estimates surface velocities and rates of frontal ablation at 27 Alaska tidewater glaciers over the period 1985–2013 and for the first time presents a time series of regional-scale frontal ablation. Using a collection of Landsat images acquired between 1985 and 2013, we apply an offset tracking algorithm to calculate fields of surface velocity for each glacier. We then use these surface velocities to iteratively constrain ice thickness using a physically based method to calculate ice thickness from surface characteristics and ice flux considerations [*Huss and Farinotti*, 2012]. We estimate frontal ablation using these surface velocity and ice thickness profiles, and in contrast to other studies that employ a fluxgate method, we adjust for both surface mass balance and ice thickness change over time and account for volume change due to changes in terminus position using previously estimated glacier lengths [*McNabb and Hock*, 2014]. We compare several commonly used approximations of frontal ablation to determine the overall effect of each approximation on the estimates of frontal ablation. Finally, we investigate the role frontal ablation plays in the regional mass budget.

2. Study Area

Glaciers in Alaska (including adjacent glaciers in the Yukon and British Columbia; hereafter "Alaska glaciers") cover a total area of 86,715 km^2 (all area estimates taken from the Randolph Glacier Inventory (RGI) v3.2 [*Pfeffer et al.*, 2014]). A total of 59 glaciers, representing approximately 13.5% of the total glacier area, have been identified as either currently or formerly tidewater [*Viens*, 1995; *Molnia*, 2008]; for this study we consider a subset of 27 glaciers that have large, active calving fronts and most likely represent the vast majority of loss due to frontal ablation in the region (Figure 1). These 27 glaciers cover approximately 11,000 km^2 (representing 96% of the total tidewater glacier area or 12.6% of the total glacier area) and range in size from 23 km^2 (Beloit Glacier) to over 3400 km^2 (Hubbard Glacier). While most tidewater glaciers in the region have retreated since the end of the Little Ice Age, many have stabilized or begun to readvance; overall, there is little coherence in the regional behavior of these glaciers [*McNabb and Hock*, 2014]. Information about individual glaciers is given in Table 1.

The three largest tidewater glaciers in the region are Hubbard, Yahtse, and Columbia, which make up ~50% of the total tidewater area. Hubbard Glacier is the largest temperate tidewater glacier in the world, at over 3400 km^2. It is also one of only a handful of Alaska tidewater glaciers that are currently advancing, which it has done since reaching its post-Little Ice Age minimum extent circa 1895 [*Trabant et al.*, 2003;

Table 1. General Statistics for Glaciers Studied[a]

Name	Area (km^2)	Number of Pairs	dL/dt ($m\,a^{-1}$)	$\bar{v}$ ($m\,d^{-1}$)	F ($Gt\,a^{-1}$)	F ($m\,w.e.\,a^{-1}$)	Flux ($Gt\,a^{-1}$)	Reg. Pct.
Hubbard	3402	282	23	2.65	3.63 ± 0.87	1.07	4.3	24.0
Yahtse	1084	142	67	3.70	1.15 ± 0.28	1.06	1.3	7.6
Columbia	944	150	−519	3.75	3.70 ± 0.89	3.92	2.6	24.5
Dawes	604	131	−62	1.75	0.54 ± 0.13	0.89	0.6	3.6
Grand Pacific	565	46	−5	0.65	0.05 ± 0.01	0.09	0.1	0.3
South Sawyer	565	153	−157	1.65	0.50 ± 0.12	0.89	0.5	3.3
Harvard	527	109	16	1.46	0.47 ± 0.11	0.90	0.6	3.1
LeConte	482	92	−30	2.85	0.96 ± 0.23	2.00	1.0	6.4
Chenega	392	100	−2	0.46	0.17 ± 0.04	0.44	0.2	1.1
Johns Hopkins	254	105	12	2.21	0.55 ± 0.13	2.16	0.6	3.6
Guyot	220	100	−111	3.28	0.66 ± 0.16	2.99	0.7	4.3
Tsaa	203	120	11	3.52	0.39 ± 0.09	1.92	0.4	2.6
Margerie	182	132	−1	0.90	0.04 ± 0.01	0.25	0.1	0.3
Turner	177	100	−58	1.73	0.30 ± 0.07	1.69	0.4	2.0
Yale	165	123	−15	1.94	0.40 ± 0.10	2.43	0.4	2.7
Northwestern	161	130	8	0.99	0.12 ± 0.03	0.76	0.1	0.8
Meares	149	89	2	1.44	0.17 ± 0.04	1.14	0.2	1.1
Tyndall	145	165	−1	1.04	0.27 ± 0.07	1.87	0.2	1.8
Sawyer	145	173	−141	0.60	0.09 ± 0.02	0.65	0.1	0.6
McCarty	119	99	−29	1.08	0.16 ± 0.04	1.34	0.2	1.1
McBride	119	58	−120	0.78	0.08 ± 0.02	0.71	0.1	0.6
Barry	106	112	−175	1.60	0.16 ± 0.04	1.48	0.2	1.0
Surprise	77	100	7	1.00	0.10 ± 0.02	1.32	0.1	0.7
Aialik	74	155	6	2.00	0.30 ± 0.07	3.99	0.3	2.0
Blackstone	68	121	3	0.79	0.03 ± 0.01	0.50	0.0	0.2
Holgate	56	146	−16	1.31	0.06 ± 0.02	1.13	0.1	0.4
Deloit	23	95	21	1.30	0.03 ± 0.01	1.41	0.0	0.2
All Glaciers	11,010				15.11 ± 3.63	1.37		100.00

[a]Glaciers are ordered by their area. Here number of pairs refers to the number of Landsat scene pairs used to derive the velocity record for the glacier, dL/dt is the mean rate of change of glacier length over the period 1985–2013 (difference in length from start to end divided by length of time period; data from *McNabb and Hock* [2014]), $\bar{v}$ is the mean surface ice velocity through the fluxgate, F is the mean rate of frontal ablation through the study period in both $Gt\,a^{-1}$ and meters water equivalent (m w.e.) a^{-1} (divided by glacier area), flux is the mean ice flux through each gate in $Gt\,a^{-1}$, and Reg. Pct. is the percentage contribution of that glacier's frontal ablation to the regional total.

Motyka and Truffer, 2007; *Ritchie et al.*, 2008; *McNabb and Hock*, 2014]. This advance, which is out of phase with most Alaska tidewater glaciers, is driven by its extremely high-accumulation area ratio of 0.95 [*Motyka and Truffer*, 2007]. *Burgess et al.* [2013] estimated that Hubbard loses about 2.7 $Gt\,a^{-1}$ to frontal ablation over the period 2007–2010, though this estimate is based on a fluxgate well upstream (~20 km) of the current terminus where surface velocities are much lower, likely leading to an underestimation of frontal ablation.

Yahtse Glacier is another of the glaciers in the region that are advancing, having done so since the mid-1980s [*McNabb and Hock*, 2014]. In that time, it has advanced over 2 km, pushing forward a moraine in relatively shallow (depth <100 m) water. Recent evidence [*Bartholomaus et al.*, 2013] suggests that a substantial portion (~50%) of the frontal ablation at Yahtse Glacier is due to submarine melting at the grounded glacier front, similar to findings at LeConte Glacier in southeastern Alaska [*Motyka et al.*, 2003, 2013].

Much has been written about the retreat of Columbia Glacier, which began circa 1980 and continues through the present [e.g., *Krimmel*, 2001; *McNabb and Hock*, 2014]. The glacier terminus has retreated over 20 km in that time, with Columbia losing over 50% of its mass and separating into dynamically distinct branches [*Meier and Post*, 1987; *Krimmel*, 2001; *O'Neel et al.*, 2005; *Rasmussen et al.*, 2011; *McNabb et al.*, 2012]. Due to this retreat, Columbia is one of the largest single contributors to sea level rise in

Alaska over the last 40 years, contributing ~6% of the total regional mass loss between 1962 and 2006 [*Berthier et al.*, 2010].

3. Data

3.1. Satellite Images

We used Landsat images to derive surface ice velocities through offset tracking. Landsat 4 (1982–1993) and 5 (1984–2013) scenes are available at 30 m resolution, while Landsat 7 (1999 to the present) and 8 (2013 to the present) images are available at 15 m resolution. We compiled a set of 3078 Landsat scenes acquired over Alaska between April 1985 and December 2013. Scenes were acquired with the Landsat 4 and 5 Thematic Mapper (TM) sensor (1984–2013), the Landsat 7 Enhanced Thematic Mapper Plus (ETM+) sensor (1999–2013), and the Landsat 8 Operational Land Imager (OLI) sensor (2013). Each scene has been georeferenced and orthorectified by the Landsat program; where needed, we manually applied corrections to the georeferencing using manually selected ground control points. These corrections were needed for fewer than 1% of the images used. Analysis of georeferencing has been performed by manually digitizing static ground features in each image, which gives an accuracy of 30 m [*McNabb and Hock*, 2014].

3.2. Glacier Outlines and Digital Elevation Models

Our ice thickness estimation algorithm requires both glacier outlines and digital elevation models (DEMs) as input. Glacier outlines mostly dating from 2009 to 2010 are taken from the RGI v3.3 [*Pfeffer et al.*, 2014], and DEMs at 30 m resolution have been compiled from Advanced Spaceborne Thermal Emission and Reflection Radiometer (ASTER) Global Digital Elevation Model (GDEM), Shuttle Radar Topography Mission (STRM), Interferometric Synthetic Aperture Radar (IFSAR), or Satellite Pour l'Observation de la Terre (SPOT) source data (for details, see *Kienholz et al.* [2014]), with an overall vertical accuracy of 8.7 m.

In order to account for changing ice thickness due to changing surface elevation at the terminus, we take the glacier surface along the fluxgate from the National Elevation Dataset (typically dating from 1940s to 1950s imagery—we assume a date of 1950) and the most recently available DEM (2000–2011) [*Kienholz et al.*, 2014], then linearly interpolate between the two. This approach fails to adequately capture seasonal variability, which can be substantial; it does, however, account for long-term trends in ice thickness change in the terminus region.

4. Methods

4.1. Surface Velocities

Surface velocities are estimated using Landsat scenes as input to an offset tracking algorithm. The offset tracking algorithm used here was developed by Mark Fahnestock (personal communication, 2012) and is based on principles first described by *Scambos et al.* [1992]. It is a MATLAB (©1984–2014 Mathworks, Inc.) script that takes a small subset (chip) of the first (source) image, then searches for a similar looking feature by taking progressive subsets (chips) within a larger search window in the second (destination) image. The correlation between each chip (source and destination) is recorded into a larger matrix of correlations. Matches are chosen by looking for peaks in the correlation matrix, of which there may be more than one. The final, accepted match is chosen based on the strength of the correlation ($r > 0.7$), the difference between correlation peaks, and the direction of the flow; that is, we discard matches found upstream (opposite direction of a general flow vector that is input to the software) of the source feature. For each glacier, Landsat images are sorted by date within sets of path/row pairs, and image pairs are chosen from images separated by between 16 and 35 days. Each Landsat scene is cropped to fit a window showing the terminus region of the glacier. These windows are chosen once for a glacier and are not resized, which means that they are large enough to account for glacier retreat and advance.

Not all of the image pairs used are completely free of cloud or shadows; even a difference in snow cover from one scene to the next can be enough to cause false correlations with the offset tracking algorithm. In order to interpolate values of surface velocity at such locations, it is necessary to introduce a filter. We are interested in the surface velocities across a cross section of the glacier (hereafter, "fluxgate"; for our purposes, an imaginary line across the glacier located upstream of the terminus through which we estimate ice flux) and we can leverage the shape of the velocity profile to reduce/remove these false correlations. First, we choose velocity fields that are free of cloud or shadow effects and calculate the dot product of the velocity field with the fluxgate normal. While the magnitudes of the velocities across this fluxgate vary through

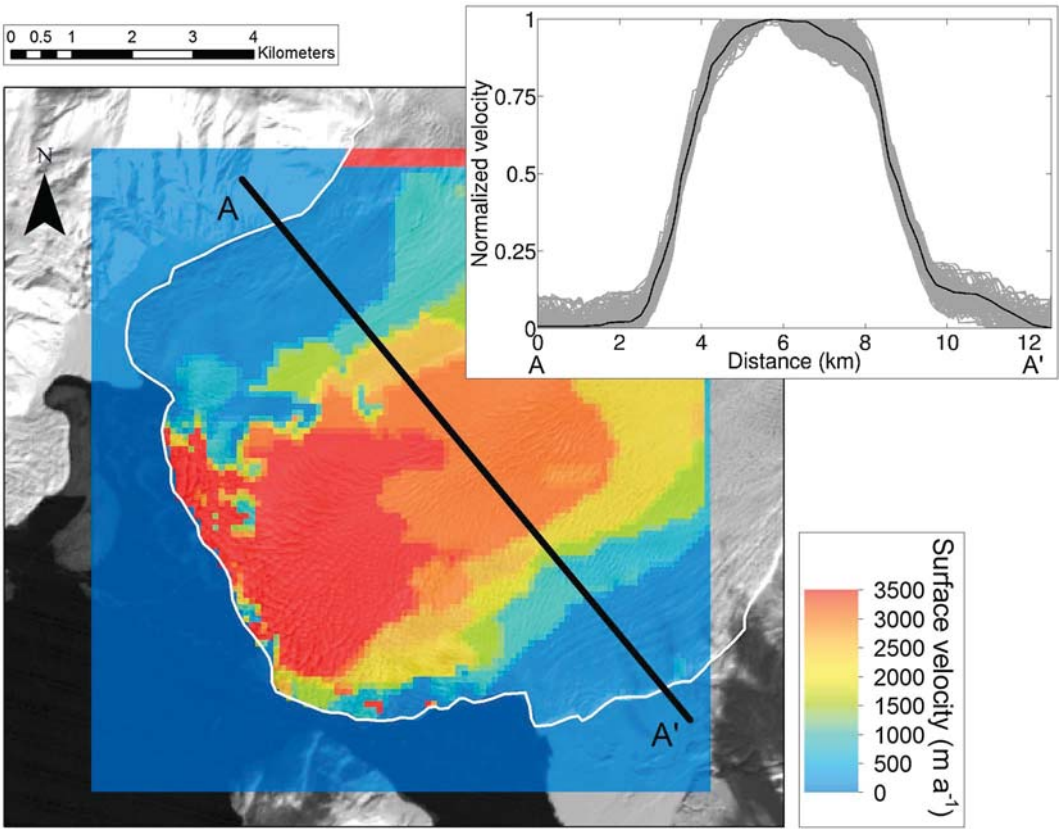

Figure 2. Surface velocity field for Hubbard Glacier, overlain on a Landsat 5 scene acquired 21 March 1995. Black line indicates the fluxgate (oriented northwest-southeast) used for Hubbard Glacier. Inset shows standard surface velocity curve for Hubbard glacier along fluxgate. Individual measurements between 1985 and 2013 are shown as gray lines; black line is the smoothed mean value for each grid point.

time, the spatial pattern of the velocity profile remains relatively constant (Figure 2). We normalize each of these velocity profiles to the maximum value for each individual curve and find the mean normalized velocity curve by averaging the normalized velocity values at each point for the set of profiles. We take this curve of mean values to be the standard velocity curve for each glacier and use it to interpolate missing values along the fluxgate for each velocity profile.

For each image pair that has cloud or shadowing effects (e.g., sharp transitions/spikes and velocity values well outside of the normal range for that glacier), we apply the following technique. First, any values along the fluxgate that indicate sharp transitions or spikes in velocity are discarded automatically based on the spatial derivative of the velocity profile. We then normalize this individual velocity curve to the maximum value along this curve and exclude values that differ from the standard velocity curve by more than 10%. Finally, we fill in the holes in this curve using the standard velocity curve found earlier and the maximum cross-sectional velocity from this profile, and smooth the final cross-sectional velocity curve with a moving average filter.

Glacier velocities, rates of frontal ablation, and terminus position vary on seasonal time scales [*Ritchie et al.*, 2008; *Moon and Joughin*, 2008; *McNabb and Hock*, 2014]. Because our data set is not evenly spaced in time, we are unable to use the entire data set to estimate these variations. To estimate seasonal variations and annually averaged rates of frontal ablation in years with more sparse measurements, we determine the average seasonal change observed throughout the time period. We initially restrict our analysis of seasonal change to only those years with four or more observations spaced throughout the year (i.e., at least three seasons). We then normalize each of these curves to its annual maximum and subtract the annual mean value. Finally, we take the monthly mean of these values in order to estimate the seasonal variations, and weight the annually averaged values for each glacier using the values of this average curve. In this way, we calculate the mean seasonal variation throughout the time period.

4.2. Ice Thickness

For Columbia Glacier, we use the bed topography and ice thickness maps calculated by *McNabb et al.* [2012], as this is the only tidewater glacier in the region that has a spatially distributed bed elevation and ice thickness data set. For the other 26 glaciers, we calculate ice thickness distribution based on the approach proposed by *Huss and Farinotti* [2012]. We have chosen this method because it requires relatively few input data to the method proposed by *McNabb et al.* [2012].

Local ice thickness is given by the inversion of volume fluxes through cross sections along the glacier relying on the principles of ice flow dynamics, using glacier outlines and DEMs as input. First, apparent surface mass balance gradients [*Farinotti et al.*, 2009] are estimated for each glacier separately to account for the effect of maritime versus continental conditions. We adopt the same model parameters as applied by *Huss and Farinotti* [2012] and do not use glacier-specific data to constrain the apparent mass balance gradient. Using an integrated form of *Glen*'s 1955 flow law for ice, the deformational component of total ice volume flux is converted to local ice thickness accounting for the effect of surface slope, varying valley shape and basal shear stress distribution along the glacier. The ice volume flux due to basal motion is approximated by prescribing a simple and constant function of sliding fraction versus glacier elevation range based on results by *McNabb et al.* [2012] for Columbia Glacier. The fraction of surface motion due to basal sliding is between 95% close to the terminus and 30% in the accumulation area. In the absence of data for other glaciers, we assume this relationship to hold for all investigated glaciers. The uncertainty associated with this assumption is likely to be small, as the model is not especially sensitive to this input. Our approach yields an estimate of ice thickness and bedrock elevation for every grid cell of the DEM and is consistent with the parameterized ice flow dynamics of each glacier.

In order to describe ice volume fluxes, and thus thickness distribution, along marine-terminating glaciers an estimate of the frontal ablation flux is required and can be prescribed in the model. Lacking any data, *Huss and Farinotti* [2012] used regional level estimates of frontal ablation for each glacier. Here we refine this approach by constraining this input using our surface velocities. As a first approximation, we assume that the glacier-wide apparent surface mass balance is zero and represents the total mass change, i.e., there is no frontal ablation.

Since the ice thickness calculation depends on ice volume flux, and hence on frontal ablation, and frontal ablation is a function of ice thickness, an iterative method is needed for refining the ice thickness estimates. We first use the initial ice thickness estimate, which assumes that no mass is lost through the glacier terminus, to calculate the rate of frontal ablation using the fluxgate approach. We then recalculate the ice thickness distribution by adapting ice volume fluxes so that they match the updated estimate of frontal ablation at the terminus and proceed until we reach a stopping point; in this case, where the change in calculated frontal ablation from one step to the next is less than 5% for each glacier. This method converged to a single value for all glaciers within four iterations (see Figure 3b). Ice thickness and bedrock topography are evaluated for one point in time (the most recently available DEM for each glacier), but changes in thickness close to the terminus over time are taken into account based on direct observations (section 3.2).

Five of the investigated glaciers (Hubbard, Columbia, Yahtse, Yale, and Harvard) have recent ice thickness measurements [*Rignot et al.*, 2013] that we can use to validate our calculated ice thickness distributions. These data were acquired in 2012 from airborne low-frequency radar and have a nominal accuracy of 17 m in ice. Comparison to calculated ice thicknesses using the initial (unconstrained) estimate for the five glaciers yields a mean difference of 145 $\pm$ 224 m; using the final, constrained ice thickness distribution reduces this to 70 $\pm$ 256 m (Figure 3). Examining the differences as a percentage of the measured ice thickness yields a mean percent difference of 21% for the initial estimate, compared to a mean percent difference of 1% for the final constrained ice thickness distribution. The median values for the percent difference are 29% and 9%, respectively; overall, our constrained ice thickness distributions provide a satisfactory approximation of the ice thickness in the region of interest.

4.3. Frontal Ablation

We define the rate of frontal ablation u_f (the sum of the calving rate u_c and the melt rate at the terminus $\dot{m}$) as the difference between the ice velocity at the terminus u_t and the rate of change of the terminus position $\partial L/\partial t$ [cf. *O'Neel et al.*, 2003; *Amundson and Truffer*, 2010]:

$$u_f(t,x,y,z) = u_c(t,x,y,z) + \dot{m}(t,x,y,z) \cdot \hat{n} = u_t(t,x,y,z) - \frac{\partial L}{\partial t}(t,x,y,z) \cdot \hat{n}, \quad (1)$$

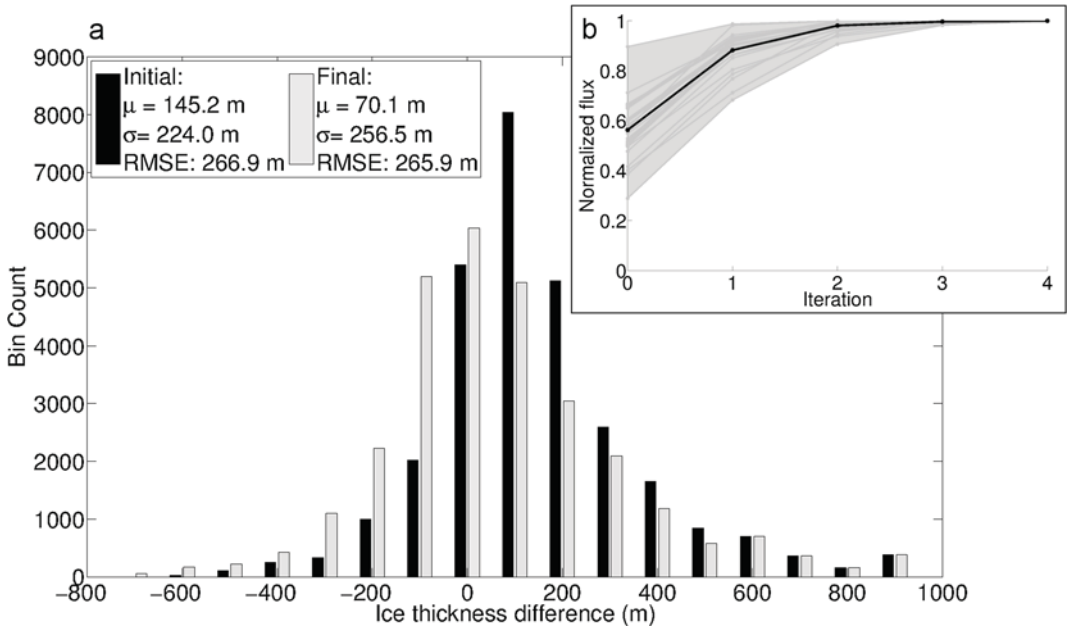

Figure 3. (a) Comparison of calculated ice thicknesses interpolated along radar tracks to measured ice thickness [*Rignot et al.*, 2013] for initial estimate (black) and final, constrained ice thickness (gray). Values for the mean (μ), standard deviation (σ), and root-mean-square error of each data set are as indicated; (b) convergence of the frontal ablation estimate and ice thickness calibration. Gray envelope indicates spread of set of glaciers; black line indicates mean value at each time step.

where $\hat{n}$ is the outward normal vector to the plane of the terminus. We choose the notation u_f because we are explicitly focusing on the mass loss at the terminus (frontal ablation), rather than only the mass lost through calving [*Cogley et al.*, 2011]. In this study, we choose to report frontal ablation as having a positive sign.

The total rate of frontal ablation F is then u_f integrated over the width of the terminus; because this surface is constantly changing, we instead integrate over a cross section (fluxgate) of the glacier, Ω, located some distance upstream of the terminus. By doing this, we must take into account mass changes due to surface mass balance ($\dot{b}$) after the ice passes through the fluxgate. For this study, we assume a value of $\dot{b} = -10$ m w.e. a^{-1}, which matches the largest values found near the termini of these glaciers [e.g., *Rasmussen et al.*, 2011]; this has the effect of placing an upper bound on the reduction in F due to surface mass balance.

Here we assign the coordinate y to be along the fluxgate. Because $\partial L/\partial t$ is not defined at Ω, we instead use the width-averaged value (i.e., calculated as by the "box method") [*Moon and Joughin*, 2008; *McNabb and Hock*, 2014], which we label $\mathrm{d}L/\mathrm{d}t$, and multiply it by the cross-sectional area of the fluxgate, A. This has the same effect as integrating $\partial L/\partial t$ over the terminus:

$$F = \iint u_f \cdot \hat{n}\ \mathrm{d}y\ \mathrm{d}z \approx \iint u_t \cdot \hat{n}\ \mathrm{d}y\ \mathrm{d}z - A\frac{\mathrm{d}L}{\mathrm{d}t} + \iint \dot{b}\ \mathrm{d}x\ \mathrm{d}y, \tag{2}$$

where we have suppressed the notation (t,y,z) for ease of reading.

The depth-averaged velocity at a given location is the integral of the vertical ice velocity profile $u(z)$ over the ice thickness H at that location:

$$\frac{1}{H}\int_H u(z)\,\mathrm{d}z = \gamma u_s, \tag{3}$$

where u_s is the surface velocity and $\gamma \in [0.8, 1]$ is a factor relating u_s to u [*Cuffey and Paterson*, 2010]. Because the ice flow near the terminus of most tidewater glaciers is primarily driven by sliding, we assume that $\gamma = 0.9$ for all glaciers in this study [*Rasmussen*, 1988; *Pfeffer*, 2007; *McNabb et al.*, 2012].

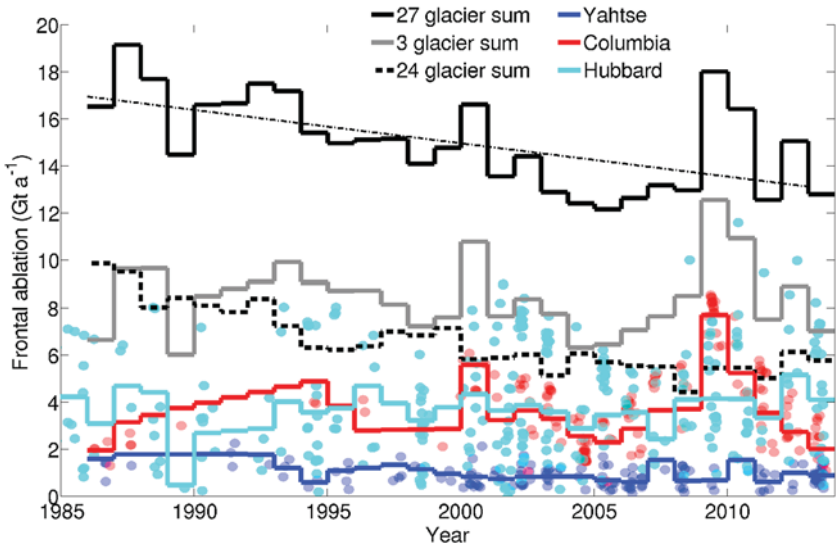

Figure 4. Time series of frontal ablation estimates for the 27 glacier sum, the 24 glacier sum, and the three glaciers with the largest rates of frontal ablation, 1985–2013.

With this, our expression for F becomes (with the dependence of F on t and the dependences of H and u_s again made explicit):

$$F(t) = \gamma \int_0^W H(t,y)\, u_s(t,y) \cdot \hat{n}\ \mathrm{d}y - A\frac{\mathrm{d}L}{\mathrm{d}t} + \dot{b}S, \tag{4}$$

where W is the width of the fluxgate and S is the glacier surface area between the fluxgate and the terminus.

For each glacier, we choose a fluxgate (Ω) well upstream of the farthest retreated terminus position and use this same fluxgate for each velocity field. *McNabb and Hock* [2014] provides a record of terminus position for all of the glaciers in this study over this time period. We calculate $L(t)$ following the box method described by *Moon and Joughin* [2008], calculating the average length between the fluxgate and the terminus; $\mathrm{d}L/\mathrm{d}t$ is then the difference in length between the first and second images used to derive the velocity field. Finally, to scale our results to the remaining nine active tidewater glaciers in Alaska, we derive and apply a linear relationship between glacier area and rate of frontal ablation.

5. Results

5.1. Frontal Ablation

Figure 4 shows a time series for the three glaciers with the largest average rates of frontal ablation, as well as the annual regional sum. In total, the 27 glaciers in the study region lost an average of 15.11 ± 3.63 Gt a^{-1} by frontal ablation over the period 1985–2013 (see section 5.2 for details on uncertainty estimation). The glacier with the highest rate of frontal ablation over the study period is Columbia Glacier, with a mean rate of 3.70 ± 0.89 Gt a^{-1}, followed by Hubbard Glacier, with a mean rate of 3.63 ± 0.87 Gt a^{-1}. These two glaciers represent approximately 50% of the frontal ablation over the time period of this study. Another two glaciers (Yahtse and LeConte) have rates of frontal ablation of approximately 0.9 Gt a^{-1} or greater; these four glaciers represent nearly 65% of the loss through frontal ablation for the 27 glaciers studied.

Figure 5 shows that, in general, glaciers with a larger area lose more mass through frontal ablation. In itself, this is not surprising, as glaciers with a larger area are generally thicker, have larger calving fronts, and have higher surface velocities. *McNabb and Hock* [2014] find 36 actively calving tidewater glaciers in Alaska; 27 of those are used in this study. The other nine glaciers are generally small, slow, and do not provide satisfactory results for offset tracking, so we apply this scaling relationship to estimate the rate of frontal ablation for the entire region. These scaled values (along with the glacier areas) are shown in Table 2. Summing the scaled estimates for the other nine glaciers yields an additional 0.45 ± 0.1 Gt a^{-1}, for a total for the region of 15.56 ± 3.73 Gt a^{-1}. The 27 glaciers that we use in this study, then, represent ~97% of the total frontal ablation from the region.

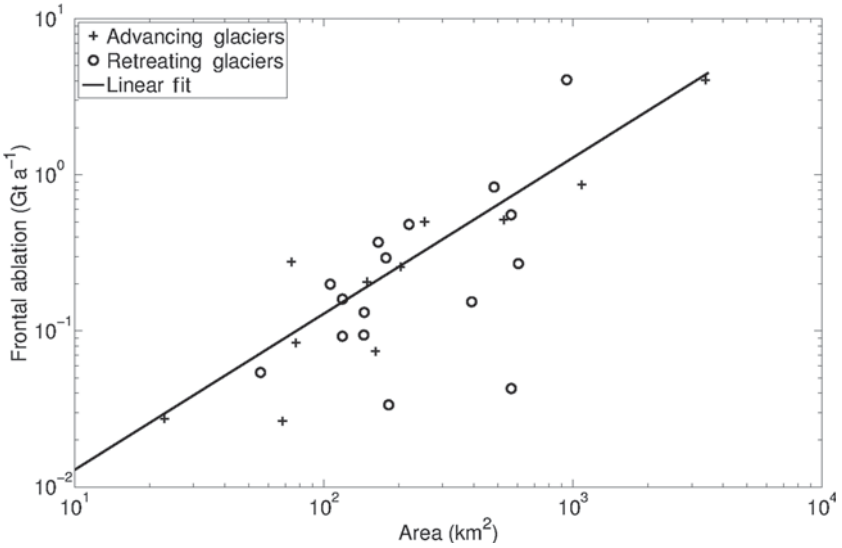

Figure 5. Frontal Ablation as a function of area for the 27 glaciers used in this study. Glaciers that advanced over the period 1985–2013 are shown as crosses, glaciers that retreated over the same time period are shown as circles. Black line indicates linear fit.

5.2. Uncertainty Analysis

Uncertainty in values of frontal ablation arises primarily from the uncertainties in values of surface velocity and ice thickness. Uncertainties in surface velocities arise from point identification in images and interpolation of irregularly spaced data to grid nodes, as well as the error in georeferencing. We use the following equation to estimate the uncertainty (in m a^{-1}) in velocities derived from Landsat imagery [cf. *McNabb et al.*, 2012]:

$$E_{\mathrm{vel}} = 365\frac{C\Delta x}{\Delta t}, \tag{5}$$

where C is uncertainty in image registration and offset tracking in pixels (p), Δx is the image resolution in m p^{-1}, and Δt is the time separation between successive images in days. Using typical values of 1 pixel for C, 30 m p^{-1} for Δx, and 32 d for Δt, we estimate an uncertainty of 345 m a^{-1} in velocity values derived from Landsat 4 and 5 scenes, and 171 m a^{-1} in velocity values derived from Landsat 7 and 8 scenes ($\Delta x = 15$ m p^{-1}). Given typical values of surface velocity averaged over cross-sectional profiles, this corresponds to a ~20% uncertainty in velocity. It may be possible to decrease this uncertainty by increasing the time span between successive images, though the corresponding change in the glacier surface characteristics would likely decrease the correlation results in the offset tracking algorithm, resulting in less certain matches.

Table 2. Frontal Ablation for the Nine Actively Calving Glaciers Not Included in the Fluxgate Analysis[a]

Name	Area (km^2)	F (Gt a^{-1})
Lamplugh	142	0.16
Nellie Juan	98	0.11
Tiger	59	0.07
Gilman	26	0.03
Coxe	20	0.02
Smith	19	0.02
Anchor	14	0.02
Grotto	11	0.01
Ogive	3	< 0.01
All glaciers	392	0.45

[a] F was derived from applying the scaling relationship shown in Figure 5.

Uncertainties in ice thickness arise primarily from errors in the thickness modeling, the glacier outlines and DEM used, and field data [*Huss and Farinotti*, 2012]. Based on comparison of modeled and measured ice thicknesses, we use the median percent difference between modeled and measured ice thickness of 10%.

Finally, uncertainties in rates of glacier length change arise primarily from errors in manual digitization of terminus outlines and errors in georeferencing of

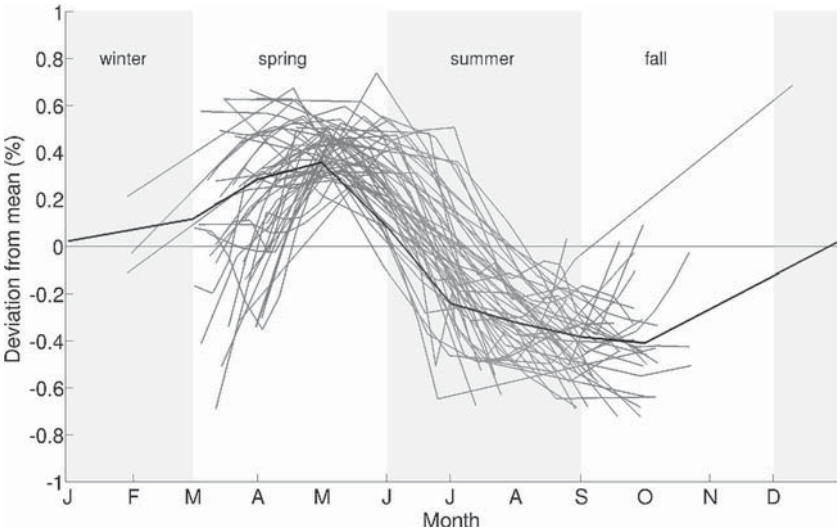

Figure 6. Normalized rates of frontal ablation with annual mean removed versus time of year, for those years where measurements are sufficiently spaced to discern seasonal signal. Black line indicates monthly mean values, interpolated for those months where no measurements are available. Mean seasonal peak is in May, with lowest values reached in September on average. Winter measurements tend to be closest to the annual average.

images [*McNabb and Hock*, 2014]. Based on results from that study, the uncertainty in annual rates of glacier length change are approximately 10%. Assuming that each of these uncertainties (surface velocities, ice thicknesses, and glacier length change) are uncorrelated, we arrive at a final estimate for uncertainty in rates of frontal ablation of 24%.

6. Discussion

6.1. Surface Velocities

Several glaciers in the region have records of ice velocity that we can compare to our values. *Trabant et al.* [2003] give centerline values of ice surface speed for Hubbard Glacier that range from 5 to 9 m d^{-1} (1800–3300 m a^{-1}) at a location near our fluxgate over the period 1980–2000, matching our range of values from 3 to 12 m d^{-1} (1100–4400 m a^{-1}) for the centerline velocity of Hubbard Glacier. *Krimmel* [2001] and *McNabb et al.* [2012] published a record of ice velocity for Columbia Glacier from 1983 to 2012, overlapping with the time period of our Landsat scenes. Differences in surface velocity from measurements at similar times are small, typically around 100–200 m a^{-1}, or 10% of the surface velocity values; this indicates that our reported uncertainty in ice velocity of 345 m a^{-1} may be an upper bound, at least for the largest glaciers.

6.2. Frontal Ablation

6.2.1. Seasonal Variation

For the years with good seasonal spacing of data (more than four measurements, spanning at least three seasons), we see that in general, the glaciers in this study lose the most by frontal ablation during the spring months (March–May), when surface velocities are at their peak annual values and ice supply to the terminus is therefore at a maximum (Figure 6).

This seasonal variation in rates of frontal ablation allows us to consider some of the proposed mechanisms driving frontal ablation throughout the year, as discussed in the literature. As surface velocities reach their maximum during the spring speedup as basal water pressures increase due to increased meltwater input at the bed [e.g., *Iken and Bindschadler*, 1986], rates of frontal ablation also increase. Penetration of meltwater into crevasses has been hypothesized as one mechanism to increase calving [*Benn et al.*, 2007], and submarine melting is increased by both elevated ocean water temperatures and convection driven by mixing of fjord water with meltwater at the terminus [*Motyka et al.*, 2003; *Bartholomaus et al.*, 2013]. Surface velocities slow later in the summer due to better developed drainage systems at the bed, air and fjord water temperatures decrease into the fall and winter, frontal ablation slows, and the glacier begins to readvance. These mechanisms are consistent with the timing of our observed seasonal variations, where frontal ablation is higher in the spring, lower in the late summer and fall, and in the middle in the winter, though further analysis would be required to confirm any individual proposed mechanism.

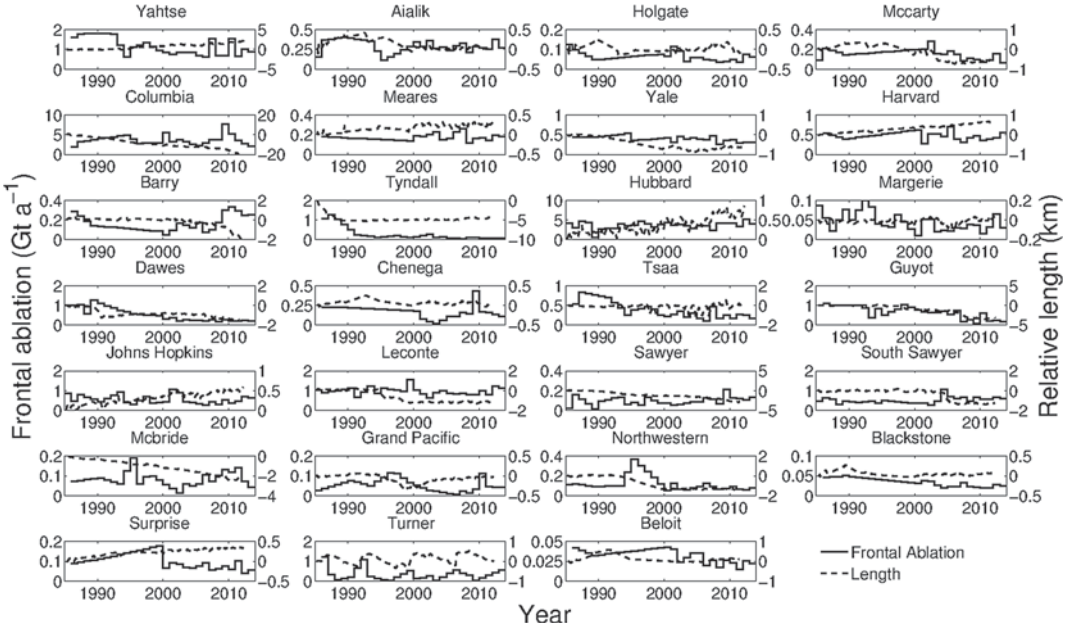

Figure 7. Frontal ablation and length versus time for the 27 glaciers used in this study. Many of these glaciers have ceased retreating and have either stabilized in shallow water or begun to readvance, explaining the apparent downward trend of frontal ablation for the region (Figure 4).

6.2.2. Interannual Variation

Figure 4 shows a trend of -0.14 Gt a^{-1} ($p < 0.01$ for the Mann-Kendall test [*Mann*, 1945]) for the regional total of frontal ablation over the time period, despite a marked increase in frontal ablation from Columbia Glacier and a slight increase from Hubbard Glacier. This negative trend comes from the remaining 25 glaciers ($p < 10^{-6}$).

Of these 25 glaciers, 16 have decreased surface velocity at the fluxgate over the time period and 18 have thinned; 11 have both slowed and thinned at the location of our fluxgate. This has occurred simultaneously with increased air and water temperatures in the region [e.g., *Royer and Grosch*, 2006; *Wendler et al.*, 2012], and increasing surface mass balance losses [e.g., *Arendt et al.*, 2006; *Johnson et al.*, 2013; *Das et al.*, 2014]. Many of these glaciers began retreating around the end of the Little Ice Age in Alaska, around the end of the nineteenth century [e.g., *Porter*, 1989; *Calkin et al.*, 2001; *Barclay et al.*, 2006, 2009; *McNabb and Hock*, 2014]. Several of these glaciers (e.g., Yahtse, Grand Pacific, Tyndall, and Harvard; Figure 7) have begun to readvance or at least appear to have stopped retreating [*McNabb and Hock*, 2014].

As these glaciers have retreated, they have depleted their mass reserves and are unable to sustain high levels of frontal ablation. Whether this is due to dynamic thinning, feedbacks from surface lowering and subsequently more negative surface mass balance, or increased submarine melt at the terminus is beyond the scope of this study; it is likely some combination of these factors, and certainly warrants further study.

Regional peaks in frontal ablation are apparent circa 2000 and 2010, due to large increases in frontal ablation from Columbia Glacier during those years. As Columbia Glacier has stopped retreating since circa 2010 [*McNabb et al.*, 2012; *McNabb and Hock*, 2014], it appears that its ability to sustain the high levels of frontal ablation since circa 1980 is nearing an end [*Colgan et al.*, 2012], most likely leaving Hubbard Glacier as the only Alaska tidewater glacier with the ability to sustain high ($\geq$3 Gt a^{-1}) levels of frontal ablation.

6.2.3. Comparison to Other Studies

A comparison of estimates of frontal ablation between this study and other published values for Alaska tidewater glaciers has been compiled in Table 3. In general, we find good agreement ($r^2 = 0.83$) with published values over the same time periods. One exception is with *Brown et al.* [1982], which does not overlap with this study. Many of the estimates from *Brown et al.* [1982] come from summer and fall, when seasonal

Table 3. Comparison of Frontal Ablation From Various Other Studies and This Study[a]

Name	Period	This Study (Gt a^{-1})	Previous Study (Gt a^{-1})	Citation
Hubbard	20 August 1977 to 1 October 1977	3.63 ± 0.87	2.24	*Brown et al.* [1982]
	2007–2010	3.41 ± 0.82	2.43	*Burgess et al.* [2013]
Yahtse	2007–2010	0.89 ± 0.21	0.99	*Burgess et al.* [2013]
Columbia	1982–2007	3.53 ± 0.85	5.5	*Rasmussen et al.* [2011]
	1983–2001	3.73 ± 0.90	3.3	*O'Neel et al.* [2005]
	1 October 1977 to 31 September 1978	3.70 ± 0.89	1.27	*Brown et al.* [1982]
Grand Pacific	August 1968 to July 1970	0.05 ± 0.01	0.02	*Brown et al.* [1982]
South Sawyer	12 July 1977 to 30 August 1977	0.50 ± 0.12	0.77	*Brown et al.* [1982]
Harvard	21 June 1978 to 1 September 1978	0.47 ± 0.11	0.24	*Brown et al.* [1982]
	2007–2010	0.36 ± 0.09	0.49	*Burgess et al.* [2013]
LeConte	2 May 1999 to 4 June 1999	0.90 ± 0.22	1	*O'Neel et al.* [2003]
Chenega	2007–2010	0.23 ± 0.06	0.37	*Burgess et al.* [2013]
Johns Hopkins	17 July 1977 to 1 September 1977	0.55 ± 0.13	0.39	*Brown et al.* [1982]
Guyot	2007–2010	0.22 ± 0.05	1.17	*Burgess et al.* [2013]
Tsaa	2007–2010	0.22 ± 0.05	0.75	*Burgess et al.* [2013]
Margerie	17 July 1977 to 1 September 1977	0.04 ± 0.01	0.06	*Brown et al.* [1982]
Turner	2007–2010	0.15 ± 0.04	0.05	*Burgess et al.* [2013]
Yale	15 July 1977 to 3 September 1977	0.40 ± 0.10	0.86	*Brown et al.* [1982]
	2007–2010	0.30 ± 0.07	0.26	*Burgess et al.* [2013]
Northwestern	2007–2010	0.07 ± 0.02	0.06	*Burgess et al.* [2013]
Meares	15 July 1977 to 3 September 1977	0.17 ± 0.04	0.12	*Brown et al.* [1982]
Tyndall	August 1964 to August 1965	0.27 ± 0.07	0.46	*Brown et al.* [1982]
	2007–2010	0.10 ± 0.02	0.11	*Burgess et al.* [2013]
McCarty	August 1964 to August 1965	0.16 ± 0.04	0.02	*Brown et al.* [1982]
	2007–2010	0.09 ± 0.02	0.12	*Burgess et al.* [2013]
Barry	2007–2010	0.20 ± 0.05	0.16	*Burgess et al.* [2013]
Surprise	2007–2010	0.05 ± 0.01	0.09	*Burgess et al.* [2013]
Aialik	2007–2010	0.25 ± 0.06	0.3	*Burgess et al.* [2013]
Blackstone	2007–2010	0.02 ± 0.01	0.08	*Burgess et al.* [2013]

[a]Time period for each comparison is given, except for *Brown et al.* [1982], where the values are compared to the period 1985–2013.

values of frontal ablation are at their lowest (cf. Figure 6), which helps explain some of the discrepancies; other glaciers were in different stages of advance/retreat during the time period of that study than the period covered here.

For only those glaciers used in both studies, *Burgess et al.* [2013] publish a total estimate of 7.32 Gt a^{-1}, compared to 6.56 ± 1.57 Gt a^{-1} for this study. *Burgess et al.* [2013] use only winter velocities, but we find this does not significantly impact estimation of frontal ablation (cf. section 6.4). Although overlapping in the error bounds, discrepancies between their estimates of frontal ablation and ours likely result from different estimates of ice thickness, because Burgess et al. used an estimation of ice thickness at the fluxgate as a function of glacier length and did not take into account the shape of the thickness profile across the gate, all of which can have a significant impact on the estimation of frontal ablation (section 6.4).

6.3. Partitioning of Mass Budget

Other studies have typically highlighted the role of frontal ablation in glacier mass budgets by quantifying the fraction of frontal ablation to total net glacier mass balance (note that the latter is the balance between total accumulation and ablation). Here we also quantify the contribution of frontal ablation to total ablation (i.e., the sum of surface ablation, which is mostly melt, and frontal ablation). To partition Alaska's glacier mass budget into its components, we compare our frontal ablation estimates to balance estimates derived from the time series of cumulative net mass balance from Gravity Recovery And Climate Experiment (GRACE) measurements for Alaska over the period 2004–2010 [*Luthcke et al.*, 2013].

We estimate the summer ablation for a given year to be the difference between the maximum and minimum values in that year [*Luthcke et al.*, 2013, Figure 8b], corresponding to a signal of ~350 Gt a^{-1} for the seven melt season between April 2004 and September 2010. Frontal ablation also occurs in each year's winter season (period between the mass minimum and following maximum) but is indistinguishable from the net mass changes in those periods because snow accumulation is the dominant component. Therefore, we simply assume that during those periods, each year's annual mean rate applies, thus adding 7 Gt a^{-1} to the summer ablation, to arrive at the annual ablation.

Our regional estimate for frontal ablation of 14 Gt a^{-1} over the same time period is then approximately 4% of the total ablation of all Alaskan glaciers, varying from year to year between 3 and 5%. The share of frontal ablation to total ablation of the tidewater glaciers alone most likely is much higher; however, surface mass balance estimates for those glaciers alone are not available to quantify this share. The contribution of frontal ablation to the corresponding total net mass change of roughly −70 Gt a^{-1} [*Luthcke et al.*, 2013] between September 2003 and September 2010 is 20%. This percentage will vary depending on the estimate for the total mass loss from Alaskan glaciers, which range from −45 Gt a^{-1} to −85 Gt a^{-1}, with a "best estimate" of −50 Gt a^{-1} [*Berthier et al.*, 2010; *Jacob et al.*, 2012; *Gardner et al.*, 2013]. Nevertheless, without frontal ablation, the mass change from Alaska glaciers would be significantly smaller, despite the seemingly negligible contribution it makes to total ablation.

Our analysis indicates that surface ablation is by far the most dominant process in removing glacier mass of Alaska's glaciers as a whole. However, frontal ablation is a significant and nonnegligible component of the regional mass budget for Alaska glaciers, despite coming from only ~14% of the glacierized area in the region.

6.4. Alternative Method Comparison

Many studies, when employing a fluxgate approach, will use some approximation of equation (4), either (1) by assuming a mean ice thickness $\bar{H}$ across the fluxgate [e.g., *Brown et al.*, 1982; *Rignot et al.*, 2008b; *Błaszczyk et al.*, 2009; *Burgess et al.*, 2013]; (2) by ignoring the volume change at the terminus through advance/retreat [e.g., *Rignot et al.*, 2008b; *Burgess et al.*, 2013]; (3) by neglecting mass loss through surface mass balance between the gate and the terminus; or (4) by using velocity measurements from only one season [e.g., *Brown et al.*, 1982; *Burgess et al.*, 2013]. In order to estimate the effects these different assumptions might have on estimates of frontal ablation, we calculate frontal ablation using our data by employing these different methods and compare the results. A full comparison of the different methods for approximating equation (4) is shown in Figure 8.

6.4.1. Neglecting Cross-Sectional Thickness Variations

Commonly, the approach of assuming a mean ice thickness $\bar{H}$ across the fluxgate takes the form

$$F(t) = \gamma \bar{u} A, \tag{6}$$

where $A = W\bar{H}$ is the cross-sectional area of the fluxgate. Rather than integrating the product $u(y)H(y)$ as in equation (4), the mean ice thickness $\bar{H}$ is multiplied by the mean surface velocity $\bar{u}$, averaged over the fluxgate. This has the effect of ignoring the shape of the bed profile (alternatively, the shape of the surface velocity profile, as $\bar{H}u(y) = \bar{u}H(y)$), which for many glaciers tends to approach a parabola or a quartic function [e.g., *Cuffey and Paterson*, 2010].

We find that ignoring the shape of these profiles leads to a substantial underestimation of frontal ablation for individual glaciers (27% on average and 17% for the regional total), almost exactly what would be expected from integrating the product of an idealized ice thickness and velocity profile. This approximation resulted in an overestimation of frontal ablation for only two glaciers (Guyot and Tsaa); our gate thickness profiles for these glaciers are nearly flat, so the product $u(y)H(y)$ is much closer to $\bar{u}\bar{H}$ for these glaciers than for more channelized glacier geometries.

6.4.2. Neglecting Terminus Advance/Retreat

Another commonly used assumption/approximation is to ignore any volume change as a result of advance or retreat of the terminus [e.g., *Rignot et al.*, 2008b]. Because advance rates tend to be much lower than retreat rates [e.g., *Post*, 1975; *Post et al.*, 2011; *McNabb and Hock*, 2014], the difference is most likely small for advancing glaciers. For rapidly retreating glaciers, however, especially those such as Columbia Glacier, this could potentially result in a significant underestimation of frontal ablation.

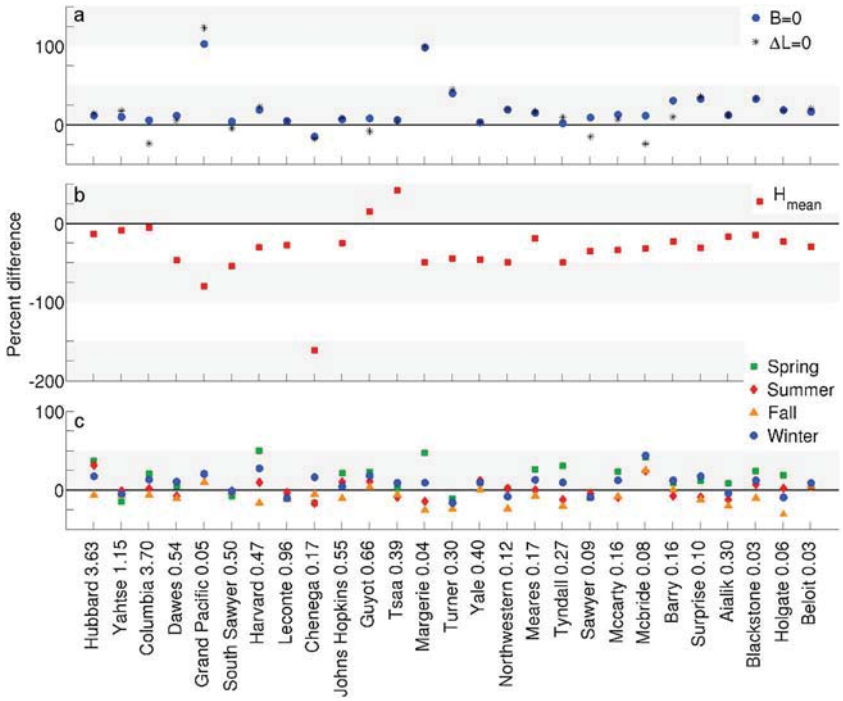

Figure 8. Difference between mean frontal ablation rates derived from four alternative methods (section 6.4) and those obtained from our approach expressed as a percent of the latter for the 27 glaciers in this study. Number following glacier name is the rate of frontal ablation for each glacier in Gt a^{-1} (Table 1). (a) $B = 0$ refers to setting surface mass balance to 0; $\Delta L = 0$ refers to ignoring length change; (b) H_{mean} refers to taking mean ice thickness instead of a profile; and (c) spring, summer, fall, and winter refer to using measurements from only those seasons, respectively.

Ignoring length change tends to overestimate frontal ablation by about 13% on average for individual glaciers in Alaska; the regional total is overestimated by only about 2%. Given the generally low rates of length change compared to surface velocity (Table 1), this relatively small value is somewhat expected. For tidewater glaciers that are not in rapid retreat (that is, most of those in Alaska), ice supply to the terminus is the dominant term of equation (4), so rates of frontal ablation are well approximated by the ice supply to the terminus alone.

6.4.3. Neglecting Surface Mass Balance Between Fluxgate and Terminus

The effect of ignoring surface mass balance between the fluxgate and the terminus when estimating frontal ablation using a fluxgate approach will necessarily depend on the distance between the fluxgate and the terminus. Surface mass balance tends to be more negative at lower elevations, meaning that ignoring it will tend to overestimate frontal ablation. In general, this seems to be quite low [e.g., *O'Neel et al.*, 2003]; for our study area, we find that neglecting surface mass balance tends to overestimate frontal ablation for individual glaciers by about 19% on average, and for the regional total about 10%. Given the relatively small areas (average of 6 km^2) between the fluxgates and the terminus, this is not surprising. The relatively small specific surface mass balance rate (a few m a^{-1}) compared to surface velocities (several hundreds of m a^{-1}) means that ice supply through the fluxgate is much larger than the surface mass balance in the area between the fluxgate and the terminus, assuming the areas over which they are integrated are similar.

6.4.4. Neglecting Seasonal Velocity and Front Variations

Alaska tidewater glaciers tend to be most advanced in the spring, and at their most retreated position in the summer and winter [e.g., *McNabb and Hock*, 2014]. Their velocities follow a similar pattern [e.g., *Krimmel*, 2001; *Ritchie et al.*, 2008], being highest in spring/early summer and lowest in the fall; therefore, rates of frontal ablation should vary seasonally. Thus, we investigate the effects of picking measurements from only one season to compute mean annual rates and compare this to results based on the collection of measurements as a whole. Because our measurement density increases dramatically after 1999, we restrict this analysis to post-1999 measurements only. Further, we define each season to be a 3 month period as follows: winter (December–February), spring (March–May), summer (June–August), and fall (September–November).

Spring measurements overestimate rates of frontal ablation by 6% on average (18% of the total), while summer and fall measurements underestimate rates of frontal ablation by 6% (8% of the total) and 14% (7% of the total) for individual glaciers, respectively. Winter measurements barely overestimated the total (1% for individual glaciers, 1% of the total), suggesting that studies such as *Burgess et al.* [2013], which exclusively use winter velocities to estimate frontal ablation, do a better job estimating annual rates of frontal ablation than do studies using measurements from summer or fall exclusively, such as *Brown et al.* [1982]. Given the difficulty in obtaining visible wavelength images during the winter in high latitudes such as the Arctic, it would be advantageous to utilize a mix of radar-based imagery, rather than relying solely on visible wavelength imagery.

7. Conclusions

Using Landsat scenes and an offset tracking algorithm, estimates of ice thickness, derived rates of length change, and a first-order estimate of surface mass balance between the fluxgate and the terminus, we present a record of frontal ablation for 27 Alaska tidewater glaciers over the period 1985–2013; to our knowledge, this is the first detailed, regional-scale, long-term study of frontal ablation for Alaska tidewater glaciers.

For the entire set of glaciers studied, we estimate a mean rate of frontal ablation of 15.11 ± 3.63 Gt a^{-1} over the period 1985–2013. Assuming a linear relationship between glacier area and frontal ablation rate, we extend this estimate to the nine other actively calving tidewater glaciers in Alaska, giving a final result of 15.56 ± 3.73 Gt a^{-1} lost through frontal ablation for Alaska tidewater glaciers. This corresponds to a specific mass loss of 1.37 m w.e. a^{-1} from tidewater glaciers alone, and a loss of 0.18 m w.e. a^{-1} from frontal ablation for all Alaska glaciers. Comparison of our estimates for individual glaciers with estimates from other studies yields general agreement; we find that large discrepancies are likely a result of differences in measurement period, using measurements from only one time of year, or a difference in method of calculating frontal ablation.

Total frontal ablation from Alaska tidewater glaciers has decreased at a rate of 0.14 Gt a^{-1} over the study period. Most Alaska tidewater glaciers began retreating at the end of the nineteenth century and have since slowed or ceased their retreats. Over the course of this study period, many glaciers have both thinned and slowed at the location of our fluxgates, likely due to some combination of dynamic thinning, increasingly negative surface mass balance, and increased submarine melting. As these glaciers have retreated, they have depleted their mass reserves and are unable to sustain high levels of frontal ablation. This depletion could have been through dynamic thinning, feedbacks from surface lowering and subsequently more negative surface mass balance, or increased submarine melt at the terminus; which of these factors is most responsible is beyond the scope of this study. Most likely, it is due to some combination of these factors, and certainly warrants further study.

We find that surface velocities and thus frontal ablation for Alaska tidewater glaciers are highly seasonal, with the seasonal amplitude averaging approximately 50% of the peak velocity, peak values occurring in late spring or early summer, and the lowest values occurring late in the summer or early fall. Any estimates of frontal ablation made using surface velocities should take this seasonal variability into consideration, though winter values are closest to the annual mean for both individual glaciers and the regional total. Ignoring the effects of cross-sectional ice thickness variations on estimates of frontal ablation tends to underestimate frontal ablation for individual glaciers by 27% (17% of the regional total), compared to 19% (10% of the regional total) overestimation from neglecting surface mass balance between the fluxgate and the terminus, and 13% (2% of the regional total) by neglecting advance/retreat of the terminus.

Our regional estimate of frontal ablation indicates the overall importance of frontal ablation in the mass budget of all Alaska glaciers. Frontal ablation constitutes 4% of the annual total ablation over the period 2003–2010, but 20% of the roughly 70 Gt a^{-1} net mass loss derived from GRACE [*Luthcke et al.*, 2013]. Without frontal ablation, the mass loss from Alaska Glaciers would be significantly reduced, despite only coming from approximately 14% of the total glacier area; this fact serves to highlight the overall importance of frontal ablation in the mass budget of regions with tidewater glaciers. The regional total of frontal ablation is heavily dominated by two glaciers in particular (Hubbard and Columbia), suggesting that regional rates of frontal ablation can be approximated by studying only a few glaciers, though with the caveat that those glaciers may not mirror regional trends.

Acknowledgments

Mark Fahnestock provided the code used to implement the offset tracking algorithm, as well as help advice in improving both the code and the manuscript. Anthony Arendt, Andy Aschwanden, Timothy Bartholomaus, Andy Bliss, Cody Beedlow, Evan Burgess, Christian Kienholz, and Shad O'Neel all provided invaluable advice and support that led to a much improved manuscript for this paper. In particular, Ed Bueler, Roman Motyka, Erin Pettit, and Martin Truffer provided insights and help in developing the ideas and methods for this study. Three anonymous reviewers provided helpful critical comments that led to the improvement of the manuscript. This work was funded in part by NSF grant EAR-0943742, NASA grant NNX11AF41G, and NASA grant NNX11A023G. Velocity and frontal ablation data will be made available through the National Snow and Ice Data Center (NSIDC).

References

Amundson, J. M., and M. Truffer (2010), A unifying framework for iceberg calving models, *J. Glaciol.*, *56*(199), 822–830, doi:10.3189/002214310794457173.

Arendt, A., K. Echelmeyer, W. Harrison, C. Lingle, and B. Valentine (2002), Rapid wastage of Alaska glaciers and their contribution to rising sea level, *Science*, *297*(5580), 382–386, doi:10.1126/science.1072497.

Arendt, A., K. Echelmeyer, W. Harrison, C. Lingle, S. Zirnheld, V. Valentine, B. Ritchie, and M. Druckenmiller (2006), Updated estimates of glacier volume changes in the western Chugach Mountains, Alaska, and a comparison of regional extrapolation methods, *J. Geophys. Res.*, *111*, F03019, doi:10.1029/2005JF000436.

Barclay, D., J. Barclay, P. Calkin, and G. Wiles (2006), A revised and extended Holocene Glacial history of Icy Bay, Southern Alaska, U.S.A., *Arct. Antarct. Alp. Res.*, *38*(2), 153–162, doi:10.1657/1523-0430(2006)38[153:ARAEHG]2.0.CO;2.

Barclay, D., G. Wiles, and P. Calkin (2009), Holocene glacier fluctuations in Alaska, *Quat. Sci. Rev.*, *28*(21-22), 2034–2048, doi:10.1016/j.quascirev.2009.01.016.

Bartholomaus, T. C., C. F. Larsen, and S. O'Neel (2013), Does calving matter? Evidence for significant submarine melt, *Earth Planet. Sci. Lett.*, *380*, 21–30, doi:10.1016/j.epsl.2013.08.014.

Benn, D. I., N. R. Hulton, and R. H. Mottram (2007), "Calving laws", "sliding laws" and the stability of tidewater glaciers, *Ann. Glaciol.*, *46*, 123–130, doi:10.3189/172756407782871161.

Berthier, E., E. Schiefer, G. K. C. Clarke, B. Menounos, and F. Rémy (2010), Contribution of Alaskan glaciers to sea-level rise derived from satellite imagery, *Nat. Geosci.*, *3*(2), 92–95, doi:10.1038/ngeo737.

Błaszczyk, M., J. A. Jania, and J. O. Hagen (2009), Tidewater Glaciers of Svalbard: Recent changes and estimates of calving fluxes, *Polish Polar Res.*, *30*(2), 85–142.

Brown, C. S., M. Meier, and A. Post (1982), Calving speed of Alaska tidewater glaciers, with application to Columbia Glacier, *U.S. Geol. Surv. Prof. Pap.*, *1258-C*, C1–C13.

Burgess, D., M. J. Sharp, D. W. F. Mair, J. Dowdeswell, and T. J. Benham (2005), Flow dynamics and iceberg calving rates of Devon Ice Cap, Nunavut, Canada, *J. Glaciol.*, *51*(173), 219–230, doi:10.3189/172756505781829430.

Burgess, E. W., R. R. Forster, and C. F. Larsen (2013), Flow velocities of Alaskan glaciers, *Nat. Commun.*, *4*, 2146, doi:10.1038/ncomms3146.

Calkin, P. E., G. C. Wiles, and D. J. Barclary (2001), Holocene coastal glaciation of Alaska, *Quat. Sci. Rev.*, *20*, 449–461, doi:10.1016/s0277-3791(00)00105-0.

Cogley, J. G., et al. (2011), *Glossary of Glacier Mass Balance and Related Terms*, IHP-VII Tech. Doc. in Hydrol., 86, UNESCO-IHP, IACS Contribution 2, Paris, France.

Colgan, W., W. T. Pfeffer, H. Rajaram, W. Abdalati, and J. Balog (2012), Monte Carlo ice flow modeling projects a new stable configuration for Columbia Glacier, Alaska, c. 2020, *Cryosphere*, *6*(2), 1395–1409, doi:10.5194/tc-6-1395-2012.

Cuffey, K. M., and W. S. B. Paterson (2010), *The Physics of Glaciers,* 4th ed., Butterworth-Heinemann, Amsterdam, Netherlands.

Das, I., R. Hock, E. Berthier, and C. S. Lingle (2014), 21st-century increase in glacier mass loss in the Wrangell Mountains, Alaska, USA, from airborne laser altimetry and satellite stereo imagery, *J. Glaciol.*, *60*(220), 283–293, doi:10.3189/2014jog13j119.

Dowdeswell, J., J. Benham, T. Strozzi, and J. O. Hagen (2008), Iceberg calving flux and mass balance of the Austfonna ice cap on Nordaustlandet, Svalbard, *J. Geophys. Res.*, *113*, F03022, doi:10.1029/2007JF000905.

Dyurgerov, M. B. (2010), Reanalysis of glacier changes: From the IGY to the IPY, 1960–2008, *Data Glaciol. Studies*, *108*, 1–116.

Enderlin, E. M., I. M. Howat, S. Jeong, M.-J. Noh, J. H. van Angelen, and M. R. van den Broeke (2014), An improved mass budget for the Greenland ice sheet, *Geophys. Res. Lett.*, *41*, 866–872, doi:10.1002/2013GL059010.

Farinotti, D., M. Huss, A. Bauder, M. Funk, and M. Truffer (2009), A method to estimate the ice volume and ice-thickness distribution of alpine glaciers, *J. Glaciol.*, *55*(191), 422–430, doi:10.3189/002214309788816759.

Gardner, A. S., et al. (2013), A reconciled estimate of glacier contributions to sea level rise: 2003–2009, *Science*, *340*, 852–857, doi:10.1126/science1234532.

Glen, J. W. (1955), The creep of polycrystalline ice, *Proc. R. Soc. London, Ser. A*, *228*(1175), 519–538, doi:10.1098/rspa.1955.0066.

Hagen, J. O., K. Melvold, F. Pinglot, and J. A. Dowdeswell (2003), On the net mass balance of the glaciers and ice caps in Svalbard, Norwegian Arctic, *Arct. Antarct. Alp. Res.*, *35*(2), 264–270, doi:10.1657/1523-0430(2003)035[0264:OTNMBO]2.0.CO;2.

Huss, M., and D. Farinotti (2012), Distributed ice thickness and volume of all glaciers around the globe, *J. Geophys. Res.*, *117*, F04010, doi:10.1029/2012JF002523.

Iken, A., and R. A. Bindschadler (1986), Combined measurements of subglacial water pressure and surface velocity of Findelengletscher, Switzerland: Conclusions about drainage system and sliding mechanism, *J. Glaciol.*, *32*(110), 101–119.

Intergovernmental Panel on Climate Change (2013), Summary for Policymakers, in *Climate Change 2013: The Physical Science Basis. Contribution of Working Group I to the Fifth Assessment Report of the Intergovernmental Panel on Climate Change*, edited by T. F. Stocker et al., pp. 1535, Cambridge Univ. Press, Cambridge, U. K., and New York.

Jacob, T., J. Wahr, W. T. Pfeffer, and S. Swenson (2012), Recent contributions of glaciers and ice caps to sea level rise, *Nature*, *482*(7386), 514–518, doi:10.1038/nature10847.

Johnson, A. J., C. F. Larsen, N. Murphy, A. A. Arendt, and S. L. Zirnheld (2013), Mass balance in the Glacier Bay area of Alaska, USA, and British Columbia, Canada, 1995–2011, using airborne laser altimetry, *J. Glaciol.*, *59*(216), 632–648, doi:10.3189/2013JoG12J101.

Kienholz, C., J. L. Rich, A. A. Arendt, and R. Hock (2014), A new method for deriving glacier centerlines applied to glaciers in Alaska and northwest Canada, *Cryosphere*, *8*(2), 503–519, doi:10.5194/tc-8-503-2014.

Krimmel, R. M. (2001), *Photogrammetric Data Set, 1957–2000, and Bathymetric Measurements for Columbia Glacier, Alaska, U.S. Geol. Surv. Water Resour. Invest. Rep., 01-4089*, Tacoma, Wash.

Larsen, C. F., R. J. Motyka, A. A. Arendt, K. A. Echelmeyer, and P. E. Geissler (2007), Glacier changes in southeast Alaska and northwest British Columbia and contribution to sea level rise, *J. Geophys. Res.*, *112*, F01007, doi:10.1029/2006JF000586.

Luthcke, S. B., A. A. Arendt, D. D. Rowlands, J. J. McCarthy, and C. F. Larsen (2008), Recent glacier mass changes in the Gulf of Alaska region from GRACE mascon solutions, *J. Glaciol.*, *54*(188), 767–777, doi:10.3189/002214308787779933.

Luthcke, S. B., T. Sabaka, B. Loomis, A. Arendt, J. McCarthy, and J. Camp (2013), Antarctica, Greenland and Gulf of Alaska land ice evolution from an iterated GRACE global mascon solution, *J. Glaciol.*, *59*, 613–631, doi:10.3189/2013JoG12J147.

Mann, H. B. (1945), Nonparametric tests against trend, *Econometrica*, *13*, 245–259, doi:10.2307/1907187.

McNabb, R., and R. Hock (2014), Alaska tidewater glacier terminus positions, 1948–2012, *J. Geophys. Res. Earth Surf.*, *119*, 153–167, doi:10.1002/2013JF002915.

McNabb, R., et al. (2012), Using surface velocities to calculate ice thickness and bed topography: A case study at Columbia Glacier, Alaska, *J. Glaciol.*, *58*, 1151–1164, doi:10.3189/2012jog11j249.

Meier, M., and M. Dyurgerov (2002), How Alaska affects the world, *Science*, *297*(5580), 350–351, doi:10.1126/science.1073591.
Meier, M. F., and A. Post (1987), Fast tidewater glaciers, *J. Geophys. Res.*, *92*(B9), 9051–9058, doi:10.1029/JB092ib09p09051.
Meier, M. F., M. B. Dyurgerov, U. K. Rick, S. O'Neel, W. T. Pfeffer, R. S. Anderson, S. P. Anderson, and A. F. Glazovsky (2007), Glaciers dominate eustatic sea-level rise in the 21st century, *Science*, *317*(5841), 1064–1067, doi:10.1126/science.1143906.
Moholdt, G., J. O. Hagen, T. Eiken, and T. V. Schuler (2010), Geometric changes and mass balance of the Austfonna ice cap, Svalbard, *Cryosphere*, *4*(1), 21–34, doi:10.5194/tc-4-21-2010.
Molnia, B. F. (2008), Glaciers of North America—Glaciers of Alaska, in *Satellite Image Atlas of Glaciers of the World*, edited by J. R. S. Williams and J. G. Ferrigno, *U.S. Geol. Surv. Prof. Pap., 1386-K*, 525.
Moon, T., and I. Joughin (2008), Changes in ice front position on Greenland's outlet glaciers from 1992 to 2007, *J. Geophys. Res.*, *113*, F02022, doi:10.1029/2007JF000927.
Motyka, R. J., and M. Truffer (2007), Hubbard Glacier, Alaska: 2002 closure of Russell Fjord and implications for future dams, *J. Geophys. Res.*, *112*, F02004, doi:10.1029/2006JF000475.
Motyka, R. J., L. Hunter, K. Echelmeyer, and C. Connor (2003), Submarine melting at the terminus of a temperate tidewater glacier, LeConte Glacier, Alaska, *Ann. Glaciol.*, *36*, 57–65, doi:10.3189/172756403781816374.
Motyka, R. J., W. P. Dryer, J. M. Amundson, M. Truffer, and M. Fahnestock (2013), Rapid submarine melting driven by subglacial discharge, LeConte Glacier, Alaska, *Geophys. Res. Lett.*, *40*, 5153–5158, doi:10.1002/grl.51011.
Nuth, C., T. V. Schuler, J. Kohler, B. Altna, and J. O. Hagen (2012), Estimating the long-term calving flux of Kronebreen, Svalbard, from geodetic elevation changes and mass-balance modelling, *J. Glaciol.*, *58*(207), 119–133, doi:10.3189/2012jog11j036.
O'Neel, S., K. A. Echelmeyer, and R. J. Motyka (2003), Short-term variations in calving of a tidewater glacier: LeConte Glacier, Alaska, U.S.A., *J. Glaciol.*, *49*(167), 587–598, doi:10.3189/172756503781830430.
O'Neel, S., W. T. Pfeffer, R. Krimmel, and M. Meier (2005), Evolving force balance at Columbia Glacier, Alaska, during its rapid retreat, *J. Geophys. Res.*, *110*, F03012, doi:10.1029/2005JF000292.
Osmanoglu, B., M. Braun, R. Hock, and F. J. Navarro (2013), Surface velocity and ice discharge of the ice cap on King George Island, Antarctica, *Ann. Glaciol.*, *54*(63), 111–119, doi:10.3189/2013aog63a517.
Osmanoglu, B., F. J. Navarro, R. Hock, M. Braun, and M. I. Corcuera (2014), Surface velocity and mass balance of Livingston Island ice cap, Antarctica, *Cryosphere*, *8*(5), 1807–1823, doi:10.5194/tc-8-1807-2014.
Pfeffer, W. T. (2007), A simple mechanism for irreversible tidewater glacier retreat, *J. Geophys. Res.*, *112*, F03S2, doi:10.1029/2006JF000590.
Pfeffer, W. T., et al. (2014), The Randolph Glacier Inventory: A globally complete inventory of glaciers, *J. Glaciol.*, *60*(221), 537–552, doi:10.3189/2014jog13j176.
Porter, S. C. (1989), Late Holocene fluctuations of the fiord glacier system in Icy Bay, Alaska, U.S.A., *Arct. Antarct. Alp. Res.*, *21*(4), 364–379, doi:10.2307/1551646.
Post, A. (1975), *Preliminary Hydrography and Historical Terminal Changes of Columbia Glacier, Alaska*, *U.S. Geol. Surv. Hyrdolog. Invest., HA-559*, Columbia Glacier, Alaska.
Post, A., S. O'Neel, R. J. Motyka, and G. Streveler (2011), A complex relationship between calving glaciers and climate, *EOS Trans. AGU*, *92*(37), 305–306.
Rasmussen, L. A. (1988), Bed topography and mass-balance distribution of Columbia Glacier, Alaska, U.S.A., determined from sequential aerial photography, *J. Glaciol.*, *34*(117), 208–216.
Rasmussen, L. A., H. Conway, R. M. Krimmel, and R. Hock (2011), Surface mass balance, thinning and iceberg production, Columbia Glacier, Alaska, 1948–2007, *J. Glaciol.*, *57*(203), 431–440, doi:10.3189/002214311796905532.
Rignot, E. (2006), Changes in ice dynamics and mass balance of the Antarctic ice sheet, *Philos. Trans. R. Soc. London, Ser. A*, *364*, 1637–1655, doi:10.1098/rsta.2006.1793.
Rignot, E., and P. Kanagaratnam (2006), Changes in the velocity structure of the Greenland Ice Sheet, *Science*, *314*(5763), 986–990, doi:10.1126/science.1121381.
Rignot, E., J. L. Bamber, M. R. van den Broeke, C. Davis, Y. Li, W. J. van de Berg, and E. van Meijgaard (2008a), Recent Antarctic ice mass loss from radar interferometry and regional climate modelling, *Nat. Geosci.*, *1*(2), 106–110, doi:10.1038/ngeo102.
Rignot, E., J. E. Box, E. Burgess, and E. Hanna (2008b), Mass balance of the Greenland ice sheet from 1958 to 2007, *Geophys. Res. Lett.*, *35*, L20502, doi:10.1029/2008GL035417.
Rignot, E., S. Jacobs, J. Mouginot, and B. Scheuchl (2013), Ice shelf melting around Antarctica, *Science*, *341*(6143), 266–270, doi:10.1126/science.1235798.
Ritchie, J., C. Lingle, R. Motyka, and M. Truffer (2008), Seasonal fluctuations in the advance of a tidewater glacier and potential causes: Hubbard Glacier, Alaska, USA, *J. Glaciol.*, *54*(186), 401–411, doi:10.3189/002214308785836977.
Royer, T. C., and C. E. Grosch (2006), Ocean warming and freshening in the northern Gulf of Alaska, *Geophys. Res. Lett.*, *33*, L16605, doi:10.1029/2006GL026767.
Scambos, T. A., M. J. Dutkiewicz, J. C. Wilson, and R. A. Bindschadler (1992), Application of image cross-correlation to the measurement of glacier velocity using satellite image data, *Remote Sens. Environ.*, *42*(3), 177–186, doi:10.1016/0034-4257(92)90101-o.
Trabant, D., R. Krimmel, K. Echelmeyer, S. Zirnheld, and D. Elsberg (2003), The slow advance of a calving glacier: Hubbard Glacier, Alaska, U.S.A., *Ann. Glaciol.*, *36*, 45–50, doi:10.3189/172756403781816400.
van den Broeke, M., J. Bamber, J. Ettema, E. Rignot, E. Schrama, W. J. van de Berg, E. van Meijgaard, I. Velicogna, and B. Wouters (2009), Partitioning recent Greenland mass loss, *Science*, *326*(5955), 984–986, doi:10.1126/science.1178176.
Van Wychen, W., D. O. Burgess, L. Gray, L. Copland, M. Sharp, J. A. Dowdeswell, and T. J. Benham (2014), Glacier velocities and dynamic ice discharge from the Queen Elizabeth Islands, Nunavut, Canada, *Geophys. Res. Lett.*, *41*, 484–490, doi:10.1002/2013GL058558.
Viens, R. J. (1995), Dynamics and mass balance of temperate tidewater calving glaciers of southern Alaska, Master's thesis, Univ. of Wash., Seattle.
Wendler, G., L. Chen, and B. Moore (2012), The first decade of the new century: A cooling trend for most of Alaska, *Open Atmos. Sci. J.*, *6*, 111–116, doi:10.2174/1874282301206010111.